Dynamic response of an array of flexural plates in acoustic medium

Kwan Kyu Park[a] and Brutus T. Khuri-Yakub
Edward L. Ginzton Laboratory, Center for Nanoscale Science and Engineering, Stanford University, Stanford, California 94305

(Received 4 March 2012; revised 1 August 2012; accepted 7 August 2012)

The dynamic response of a transducer array made up of circular flexural plates in immersion is analytically calculated. The calculation method includes three steps: (1) the calculation of parallel resonant frequency and the velocity profile of each plate, (2) the calculation of mutual acoustic impedance between the plates, and (3) the calculation of velocity response, including the mechanical and acoustic impedance. The calculation method is validated by both finite element analysis and measurement results of a fabricated capacitive micromachined ultrasonic transducer. Based on the calculated velocity, the near-field pressure and the near-to-far field radiation patterns are presented. The flexural plate array in immersion displays two modes of operation. At low frequency, the mode shape of the transducer array is similar to that of a suspended plate and, at certain frequencies, two groups of plates move in opposite phase, which results in the cancellation of the average velocity. At high frequency, the mode shape is similar to that of a piston transducer; however, the near-field pressure distribution is similar to that of a resilient disk.
 [http://dx.doi.org/10.1121/1.4747613]

PACS number(s): 43.38.Ar, 43.38.Bs, 43.38.Hz, 43.40.Dx [TDM] Pages: 2292–2303

I. INTRODUCTION

Acoustic impedance is one of the key parameters of acoustic transducers as it is directly translated into the efficiency of acoustic transducers. In the case of a transducer array used to generate a directional sound wave, the interaction between each transducer unit introduces additional acoustic impedance which is defined as mutual acoustic impedance. The effect of the mutual acoustic impedance is significant, especially when the transducers radiate sound into a liquid medium.[1] Since Pritchard[2] presented the calculation method of the mutual acoustic impedance of circular piston transducers, the mutual acoustic impedance has been investigated on different transducer configurations, including rectangular pistons,[3] spheres,[4] and flexural disks.[5] Based on these theoretical backgrounds, focusing on the calculation method of the mutual impedance of two transducers, Lee recently introduced the lumped acoustic impedance of a piston transducer array and the optimal parameters of the array design.[6]

The mutual acoustic impedance has a significant impact on flexural mode transducers, such as piezoelectric micromachined ultrasound transducers (PMUTs), and capacitive micromachined ultrasonic transducers (CMUTs). Compared to piston transducers, the flexural mode transducers have much lower mechanical impedance with respect to the liquid medium. Thereby, the medium properties and the operating frequency highly affect the velocity profile of the plate.[7] Accordingly, the change of the velocity profile results in different acoustic impedance of the transducer.[8] Therefore, both the velocity profile of the plate and the mutual acoustic impedance affect the behavior of flexural mode transducers. Ballandras investigated the response of a periodic structure consisting of an infinite number of plates by using finite element analysis (FEA) and presented that the mutual acoustic impedance takes an important role in the dynamic response of the transducer array (i.e., a multi-plate transducer).[9] Recently, several researches have been performed on arrays of flexural mode transducers by investigating CMUTs. Caronti[10] reported FEA results on a 1-D CMUT array and presented that the mutual acoustic impedance through the liquid represented a major source of the cross coupling. Senlik[11] focused on the lumped acoustic impedance of CMUTs with several design parameters. Meynier[12] presented the analytic calculation of CMUTs, having a periodic pattern of plates.

This paper presents the analytic calculation method and its results by modeling the CMUTs of arbitrary configuration. The results of the calculation are the dynamic response of each plate of the CMUT and the pressure distribution of the multi-plate transducer with an arbitrary configuration. In Sec. II, the definitions of the model are set forth. They are followed by the calculation of the velocity profile of each plate. The calculation method of dynamic response is presented based on the calculated velocity profile. In Sec. III, the velocity response of the CMUT is presented. The calculation method is validated by FEA and the measurement of fabricated devices. In Sec. IV, the pressure distribution of the CMUT is presented and compared to that of the piston transducer. The general aim of this paper is to provide a full description of the calculation of the frequency response of CMUTs, including mutual acoustic impedance, and to present the differences between the CMUTs and the piston transducers in dynamic response and pressure field.

[a]Author to whom correspondence should be addressed. Electronic mail: kwankyup@stanford.edu

 0001-4966/2012/132(4)/2292/12/$30.00

II. MODELING OF MULTIPLE FLEXUTAL PLATES

A. Definition of Problem

The dynamic behaviors of flexural mode transducers are highly dependent on the mechanical properties of the transducers, as well as acoustic boundary conditions. Therefore, the definition of the problems with appropriate transducers' properties and acoustic boundary conditions should be introduced. This paper is based on the following assumptions, which are valid in the case of typical flexural mode transducers.

(1) A unit transducer array is made of circular plate transducers, which are located in a rigid baffle. The dimensions of all plates are identical.
(2) All plates are actuated by uniformly distributed electrostatic pressure. The excitation pressure on plates are in the same magnitude and phase.
(3) The top side of the plates is loaded by uniformly distributed acoustic pressure from the medium.
(4) A unit plate operates as a flexural mode transducer with a clamped edge. The velocity profile of the plate is axial symmetric and is only dependent on the operating frequency.

B. Velocity profile of single plate

Based on the assumptions noted prior, the velocity profile of the plate is modeled as[5]

$$u(r_0,t) = U \cdot e^{i\omega t}\left[\sum_{n=0}^{\infty} \alpha_n \left(\frac{r_0}{r}\right)^n\right], \quad r_0 \le r, \tag{1}$$

where r_0 is the point of interest and r is the radius of the plate. Consequently, the axial symmetry and the clamped-edge condition introduce:

$$u(r_0 = r) = 0, \quad \sum_{n=0}^{\infty} \alpha_n = 0, \tag{2}$$

$$\frac{u(r_0 = 0)}{\partial r_0} = 0, \quad \sum_{n=1}^{\infty} n\alpha_n \left(\frac{r_0}{r}\right)^{n-1} = 0; \tag{3}$$

where n is an even number due to the symmetry of the plate. However, the variation of the velocity profile should be considered, especially when the model is calculated in a wide range of frequency higher than the first harmonic frequency.

Figure 1(a) represents the velocity profile of a circular plate in a fluid as a function of the operating frequency. According to Senlik,[11] the velocity profile is dependent on the ratio between the operating frequency, f, and the parallel resonant frequency, f_p, at which point the average displacement of the plate becomes minimum (see appendix). In this paper, Eq. (1) is simplified into an eighth order polynomial, which is a trade-off between the error of fitting and computation time. The velocity profile coefficients, α_n, are extracted from the FEA by least-square fitting [Fig. 1(a)]. When α_0 is 1, the extracted four α_n as a function of frequency are shown in Fig. 1(b). It is useful to express α_n as a polynomial for future use as in

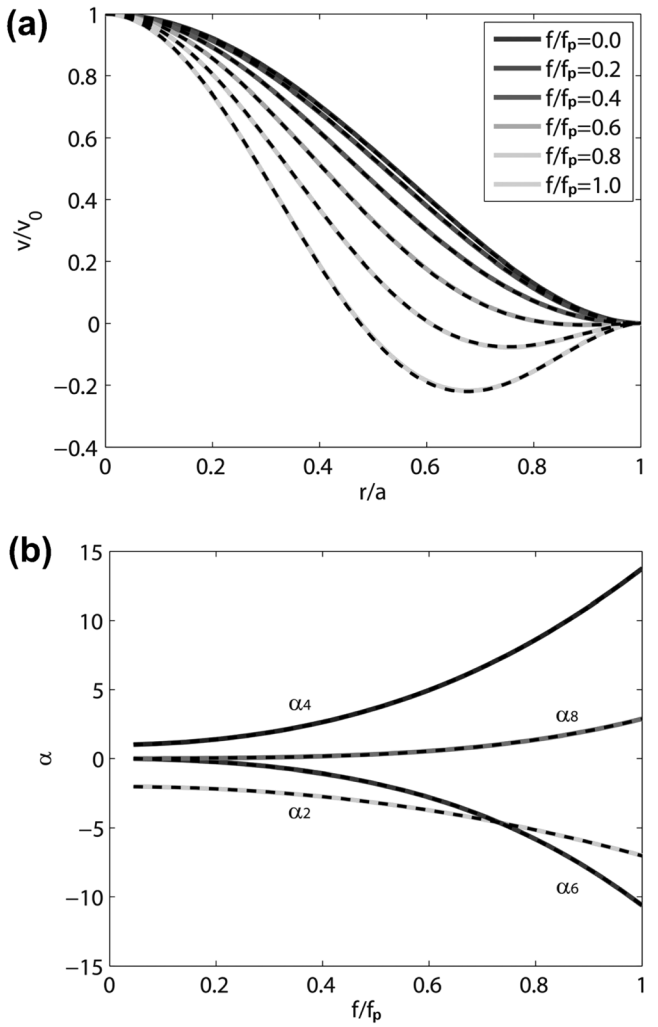

FIG. 1. (a) The mode shape of a circular plate in different frequency. The solid lines represent the extracted mode shape from FEA and the dotted lines are plotted based on the mode shape coefficient, α_n. (b) α_n as a function of frequency. $\alpha_0 = 1$ in all frequency range. Dotted lines are fitted curves based on $\beta_{m,n}$ in Table I.

$$\alpha_n = \beta_{0,n} + \beta_{1,n} f_{\text{ratio}} + \beta_{2,n}(f_{\text{ratio}})^2 + \beta_{3,n}(f_{\text{ratio}})^3, \quad f_{ratio} = \frac{f}{f_p}. \tag{4}$$

The coefficients $\beta_{m,n}$, are listed in Table I.

It should be noted that the calculation of f_p is important to estimate the velocity profile of the plate. In the case of the plate in air, f_p is close to the second harmonic frequency. When the plate is immersed in a fluid, the acoustic loading affects the dynamics of the plate. In this case, the f_p is calculated by the FEA[11] or by an analytic method as proposed in this paper (see the appendix).

TABLE I. The coefficients of the polynomial ($\beta_{m,n}$) in Eq. (4).

	$\beta_{0,n}$	$\beta_{1,n}$	$\beta_{2,n}$	$\beta_{3,n}$
α_0	1	0	0	0
α_2	−2.0166	0.2093	−4.9145	−0.3063
α_4	0.9936	0.2194	7.8718	4.7024
α_6	0.0681	−1.119	−0.8184	−8.7557
α_8	−0.0451	0.6922	−2.1462	4.3693

C. Acoustic impedance

The acoustic radiation impedance of a circular plate in a rigid baffle with various velocity profiles was introduced by Porter.[5] The self-radiation impedance, referred to the average normal surface velocity, (Z_{11}) of the velocity profile in Eq. (1) is

$$\frac{Z_{11}}{Z_0}=\frac{(kr)^2}{2\left(\sum\frac{\alpha_n}{n+2}\right)^2}\sum_{\kappa}\sum_{l}\alpha_\kappa\alpha_l\sum_{\tau=0}^{\kappa/2}\sum_{s=0}^{l/2}\times\left\{D_{\tau\kappa}D_{sl}\int_0^{\pi/2+\infty}\frac{J_{\tau+1}(kr\sin\theta)J_{s+1}(kr\sin\theta)\sin\theta}{(kr\sin\theta)^{r+s+2}}d\theta\right\}, \tag{5}$$

$$D_{\kappa m}=\left[(-1)^\kappa\frac{2^\kappa(m/2)!}{(m/2-\kappa)!}\right],\quad k=\frac{2\pi}{\lambda}=\frac{2\pi f}{c},\quad Z_0=\rho\cdot c, \tag{6}$$

where ρ and c are the density and the speed of sound of the medium, respectively. When there is more than one plate which generates sound to the surrounding medium, the acoustic radiation impedance of one plate is affected by its neighboring plates. Consider two plates which are separated by a center-to-center distance of d, then the acoustic impedance of the first plate is defined as

$$Z_{\text{acoustic},1}=Z_{11}+Z_{12}\cdot\frac{v_2}{v_1}, \tag{7}$$

where v_i is the averaged velocity of the ith plate based on volume displacement ($v_i=\int_0^r 2\pi r_0 u_i dr_o/\pi r^2$), and Z_{12} the represents mutual acoustic impedance between two plates. The closed form of the mutual acoustic impedance of the piston transducer was derived by Pritchard.[2] Later, Porter[5] extended the equation for circular flexural plates in semi-infinite series form as

$$Z_{12}(kr,kd)=R_{12}(kr,kd)+i\cdot X_{12}(kr,kd)$$

$$\frac{R_{12}}{Z_0}=\frac{(kr)^2}{2\left(\sum\frac{\alpha_n}{n+2}\right)^2}\sum_{\kappa}\sum_{l}\alpha_\kappa\alpha_l\sum_{\tau=0}^{\kappa/2}\sum_{s=0}^{l/2}\left\{D_{\tau\kappa}D_{sl}\int_0^{\pi/2}\frac{J_{\tau+1}(kr\sin\theta)J_{s+1}(kr\sin\theta)J_0(kd\sin\theta)\sin\theta}{(kr\sin\theta)^{r+s+2}}d\theta\right\},$$

$$\frac{X_{12}}{Z_0}=\frac{1}{i}\frac{(kr)^2}{2\left(\sum\frac{\alpha_n}{n+2}\right)^2}\sum_{\kappa}\sum_{l}\alpha_\kappa\alpha_l\sum_{\tau=0}^{\kappa/2}\sum_{s=0}^{l/2}\left\{D_{\tau\kappa}D_{sl}\int_{\pi/2}^{\pi/2+i\infty}\frac{J_{\tau+1}(kr\sin\theta)J_{s+1}(kr\sin\theta)J_0(kd\sin\theta)\sin\theta}{(kr\sin\theta)^{r+s+2}}d\theta\right\}. \tag{8}$$

It is important to note that Eq. (5) is a subset of Eq. (8), when $d=0$. Equation (7) can be extended for a large number of plates. For a transducer array with N plates, the total acoustic radiation impedance of ith plate is[3]:

$$Z_{\text{acoustic},i}=\sum_{m=1}^{N}Z_{im}\cdot\frac{v_m}{v_i}, \tag{9}$$

where $Z_{\text{acoustic,i}}$ is the acoustic radiation impedance of the ith plate, which has $(N-1)$ neighboring plates.

D. Dynamics of multiple plates

Calculation of the dynamic response of each plate is calculated based on the acoustic radiation impedance and the acoustic impedance of the plate. When a harmonic pressure, P is applied on the ith plate, the average velocity of the plate can be calculated as

$$P_i=Z_{\text{total},i}\cdot v_i=(Z_{\text{acoustic},i}+Z_m)\cdot v_i=\left(\sum_{m=1}^{N}Z_{im}\cdot\frac{v_m}{v_i}+Z_m\right)\cdot v_i, \tag{10}$$

where Z_m is a acoustic impedance of the plate. In this paper, Z_m is calculated using the equation derived by Mason[13] (see the appendix). Equation (10) presents that all the velocities of N plates are coupled to each other. Therefore, the velocity of all plates should be calculated simultaneously as:

$$\begin{pmatrix}P\\P\\P\\P\end{pmatrix}=Z_m\begin{pmatrix}1&&&\\&1&&\\&&\ddots&\\&&&1\end{pmatrix}\begin{pmatrix}v_1\\v_2\\\vdots\\v_N\end{pmatrix}+\begin{pmatrix}Z_{11}&Z_{12}&\cdots&Z_{1N}\\Z_{21}&Z_{22}&&\\\vdots&&\ddots&\\Z_{N1}&&&Z_{NN}\end{pmatrix}\begin{pmatrix}v_1\\v_2\\\vdots\\v_N\end{pmatrix}. \tag{11}$$

Please note that P and Z_m are identical to all plates as defined. Additionally, Eq. (11) should be calculated at each frequency, since Z_m, Z_{ij} are functions of frequency. The calculated v_i as a function of frequency presents the behavior of the transducer in a wide range of frequency.

III. VELOCITY RESPONSE

This section reports on the velocity response of a multi-plate transducer. Two devices were designed and the velocity of an individual plate and the lumped velocity of all plates were calculated. The calculated results were compared

TABLE II. The dimensions and the material properties of the plate and the medium used in the analytic calculation of design A and design B.

Description	Symbol	Value
Plate material		Stressed Silicon
Plate radius	r	21 μm
Plate thickness	t	0.5 μm
Young's modulus of plate	E	433.6 GPa
Plate density	ρ_m	
Poisson's ratio of plate	ν	0.1773
Plate-to-plate pitch	d	25 μm
Medium		Water
Speed of sound of medium	c	1500 m/s
Density of medium	ρ	1000 kg/m^3

to the results from FEA for validation. Additionally, the calculated results were compared to the measured displacement of a fabricated device.

A. Device description

Arrays of micro-fabricated circular plates immersed in water were considered in this calculation; the properties of the clamped-edge plates and the medium are presented in Table II. Two transducer arrays consist of the silicon plates, which are close-packed in hexagonal distribution; the first and the second transducer arrays are made of 19 plates (design A) and 169 plates (design B), respectively; as shown in Figs. 2(a) and 2(b).

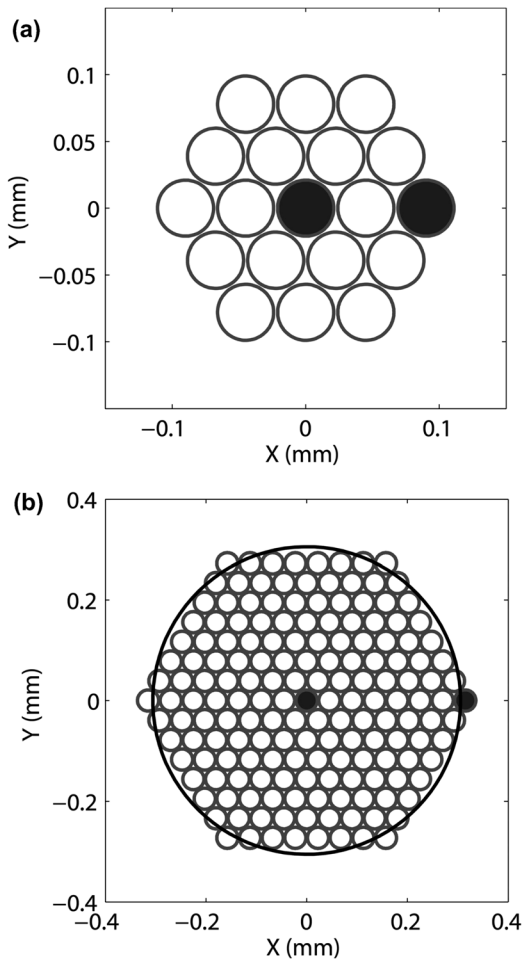

FIG. 2. Diagrams presenting the location and the radius of the plates in (a) design A and (b) design B. The center plate and the corner plate are indicated as filled circles. The biggest circle in Fig. 2(b) represents the effective radius of the array of the plates.

B. Velocity response

The average velocity responses of the plates of the two devices were calculated using Eq. (11). In order to solve (11), Z_m and Z_{ij} at each frequency should be precalculated. Z_m was calculated based on the material properties in Table II and Eq. (A1) in the appendix. Z_{ij} was calculated by using Eq. (8) and the location of plates as shown in Fig. 2. The calculated υ_i, as a function of frequency, is plotted in Fig. 3. It is impractical to plot the frequency response of all the plates but, for easier interpretation, three velocity responses were selected: the velocity response of the center plate, the corner plate, (depicted in Fig. 2), and the average velocity of all plates. Based on the pattern of the frequency response, two operation regions were observed. In the low frequency range (up to 2.5 MHz) the amplitude and phase of the average velocity of

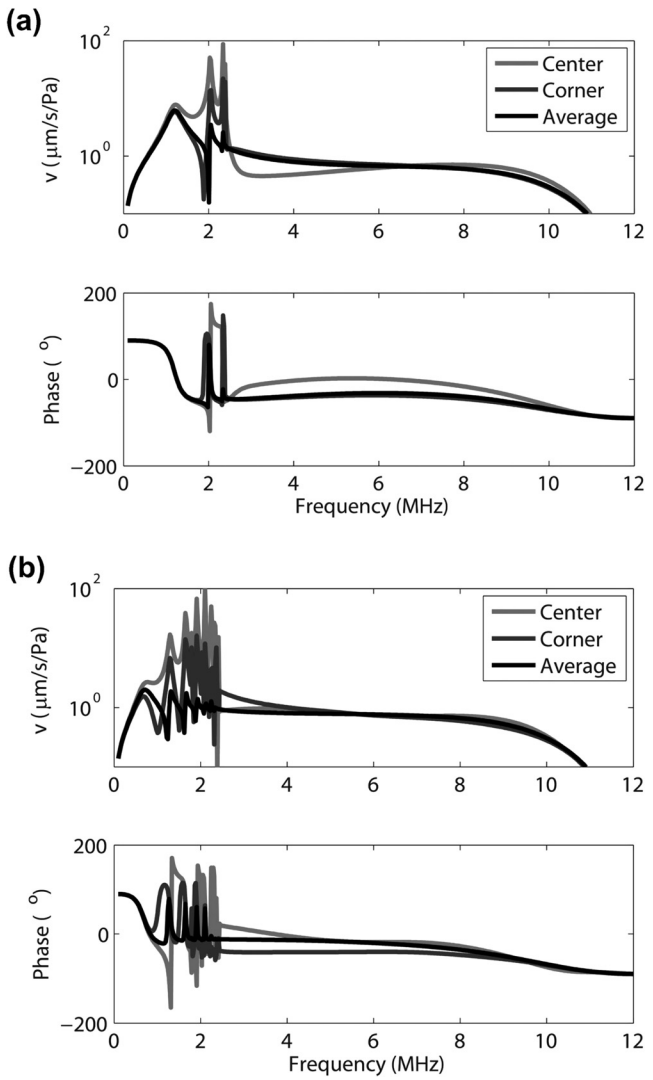

FIG. 3. The velocity response of (a) design A and (b) design B in the amplitude and phase.

each plate exhibit large variations at some frequency. In this "flexible-transducer mode," the plate velocities cancel out each other and local minima of the average velocity are observed at specific frequencies. In design A, the minimum located at 2.01 MHz, whereas in design B, minima are located at 1.25 MHz, 1.63 and 1.89 MHz. Above 2.5 MHz, the amplitude and phase of the velocity of the plates present gradual changes as functions of the frequency and do not introduce any cancellation in the average velocity. This "inflexible-transducer mode" holds to the parallel resonant frequency (f_p), 12 MHz, at which all $v_i = 0$.

The calculated results were validated by FEA. The FEA of the CMUT was performed using the commercial package COMSOL (Version 4.2a, COMSOL, Inc., Burlington, MA). The CMUT plates and the medium on top of the plates are included in the FEA model and calculated by the "Acoustic-Solid Interaction, Frequency Domain (acsl)" module. The medium was in the shape of a trimmed hemisphere and covered all plates. The mesh size of the medium was less than 1/10 of the sound wavelength at the frequency of interest. The mesh size of the plate was less than 1/10 of the plate radius. The FEA of the CMUT required a lot of computation power. The FEA model for design B has 2.8 million meshes, which generated 6.7-million degree-of-freedom equations. The typical computation time was 5880 s at each frequency, which was 200 times more than that of the analytic calculation (Intel Xeon, 3.3 GHz quad core CPU, 32 GB memory).

The average velocities of all plates in device A and B are extracted from FEA and compared to those of analytic the calculation, as shown in Fig. 4. The average velocity response agrees well with the result from FEA in terms of (1) the frequency of the local maxima and the local minima of the average velocity, (2) the magnitude of the maximum velocity, and (3) the magnitude of the average velocity in the inflexible-transducer mode (4∼8 MHz). Additionally, the transition from the flexible-transducer mode to the inflexible-transducer mode is also observed in the FEA results.

The snapshots of the displacement results of FEA clearly show the difference between the flexible-transducer

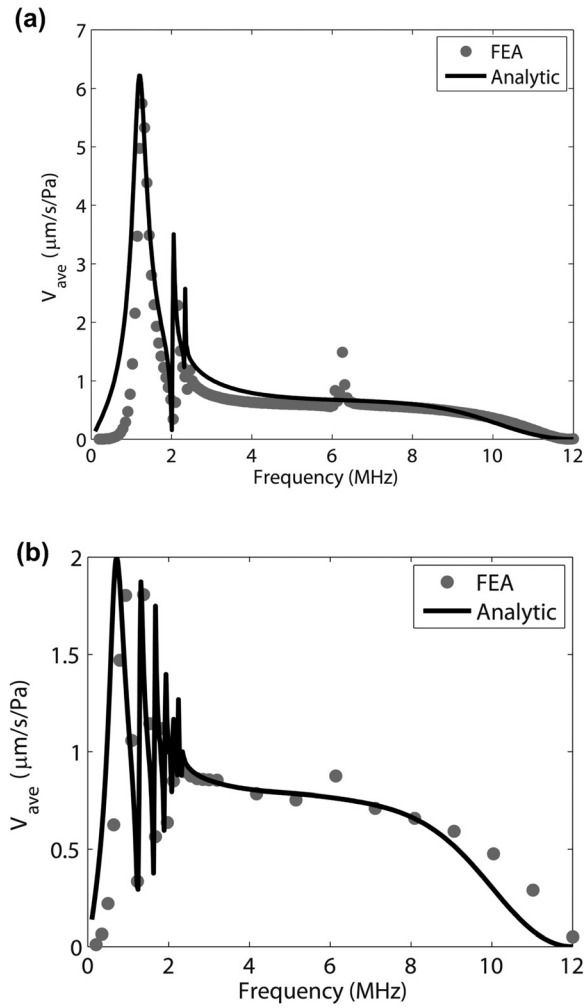

FIG. 4. The comparison of the average velocity of plates between the analytic calculation and FEA results: (a) design A, (b) design B.

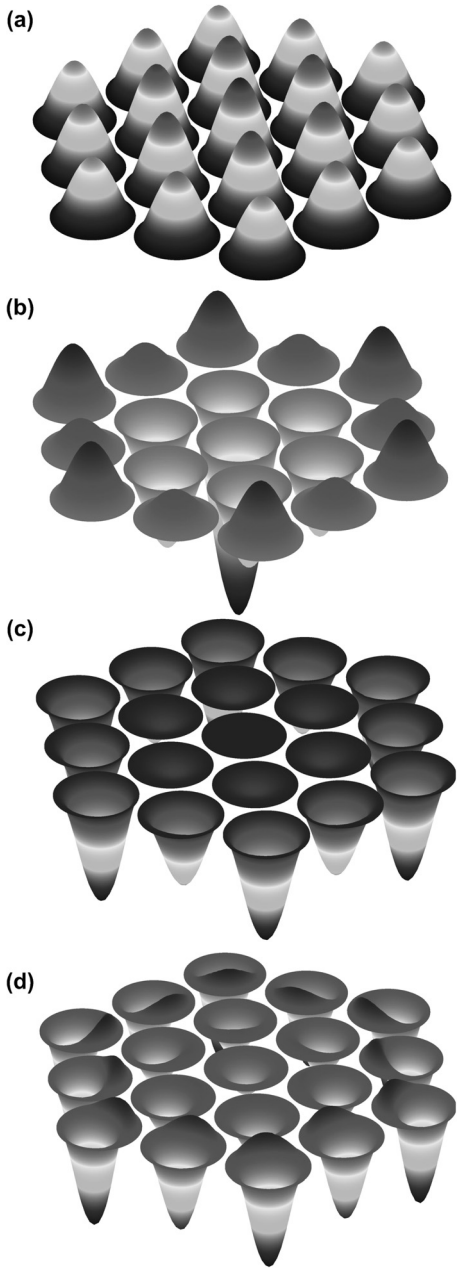

FIG. 5. The snapshot of the displacement of the design A calculated from FEA in several frequencies: (a) 1.26 MHz, (b) 2.038 MHz, (c) 4.05 MHz, and (d) 8.02 MHz.

mode and the inflexible-transducer mode; in the flexible-transducer mode [Figs. 5(a), 5(b), 6(a), 6(b), and 6(c)], the mode shape of the transducer array is similar to that of a suspended hexagonal plate. At specific frequencies in the flexible-transducer mode [Figs. 5(b), 6(b), and 6(c)], two groups of plates are moving in opposite phase, and, thus, resulting in cancellation of the average velocity, as shown as local minima in Fig. 4. In the inflexible-transducer mode [Figs. 5(c), 5(d), and 6(d)], all the plates are categorized into two groups: inner plates and edge plates. Only the plates located at the edge of the transducer have different phase compared to other plates, i.e., inner plates. As shown in Fig. 3, the inner plates and the edge plates have a difference in phase of less than 40° and have the velocities of the similar order of magnitude above 4 MHz. To be concise, the whole transducer array is moving together, except the small phase delay of the edge plates in the inflexible-transducer mode.

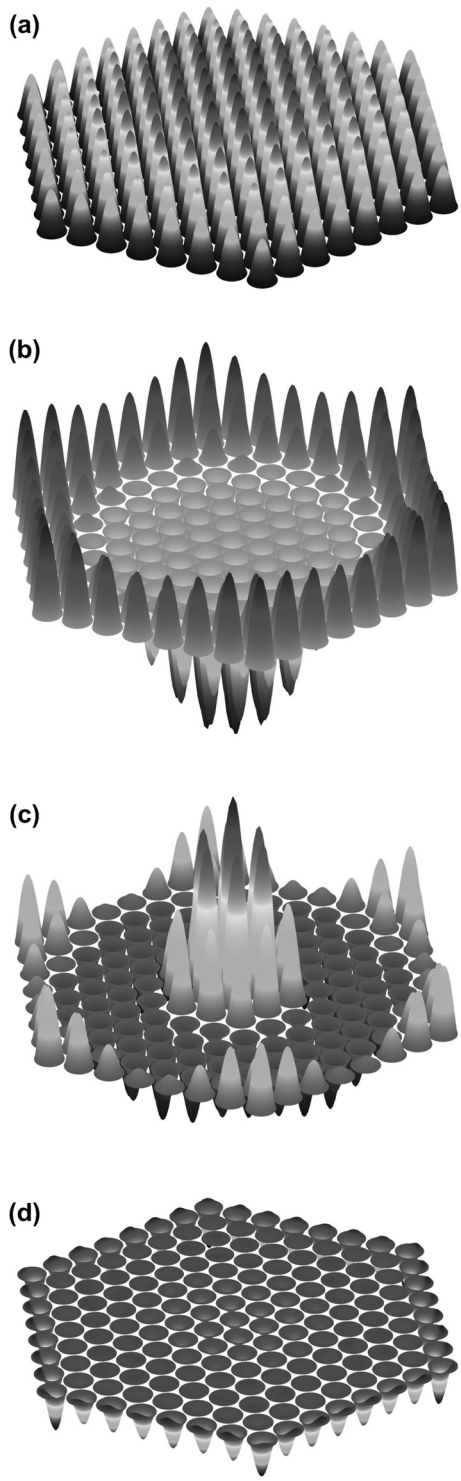

FIG. 6. The snapshot of the displacement of the design B calculated from FEA in several frequencies: (a) 0.789 MHz, (b) 1.232 MHz, (c) 1.674 MHz, and (d) 5.16 MHz

C. Displacement measurement

One of the purposes of having the model include the analytic calculations and the FEA methods discussed in this paper is to help estimate the performance of the transducer in the design phase. Therefore, it is informative to validate the calculation result by measuring the dynamic response of the actual device; CMUTs were selected for the measurement for this purpose. The CMUTs agree with the assumption in Sec. II;[14] the CMUTs consist of many flexural plates, which are closely packed together. The edge of each plate is clamped to a substrate, i.e., a rigid baffle. All plates are electrically connected and actuated by a capacitive force; therefore, the same forces in the amplitude and phase are applied on all plates. The detailed descriptions of the CMUT are well presented by Ergun.[15]

The device is fabricated by the LOCOS/wafer-bonding process[16] to realize the design B as shown in the previous section. In the fabrication process, the thin silicon plate is bonded on silicon dioxide structures which have pre-defined cavities, as shown in Fig. 7(a). The configuration of the pre-defined cavity is in a circular shape to realize the circular plate, thereby fulfilling the requirements in Sec. II A. A single transducer unit (an element) is made up of several plates, distributed in a hexagonal configuration, as shown in Fig. 7(b). By applying AC voltage superposed on DC bias voltage between the plate and the silicon substrate, all the plates are actuated by capacitive forces of the same amplitude and

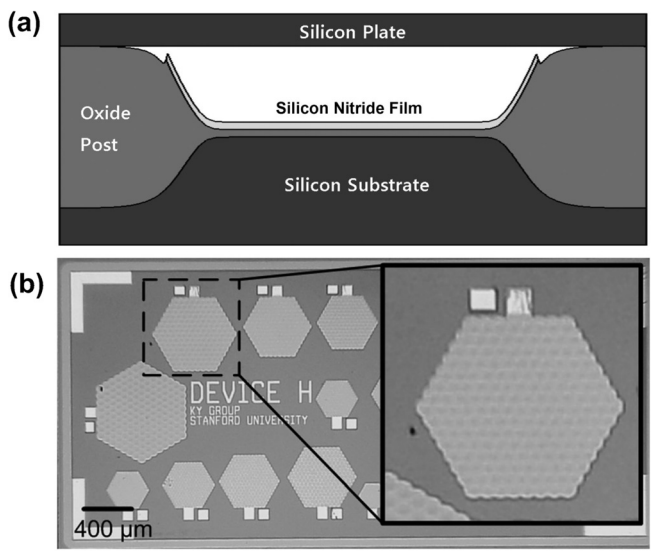

FIG. 7. (a) Cross-sectional schematic of a single circular plate in the CMUT. (b) The optical picture of a device for the displacement measurement.

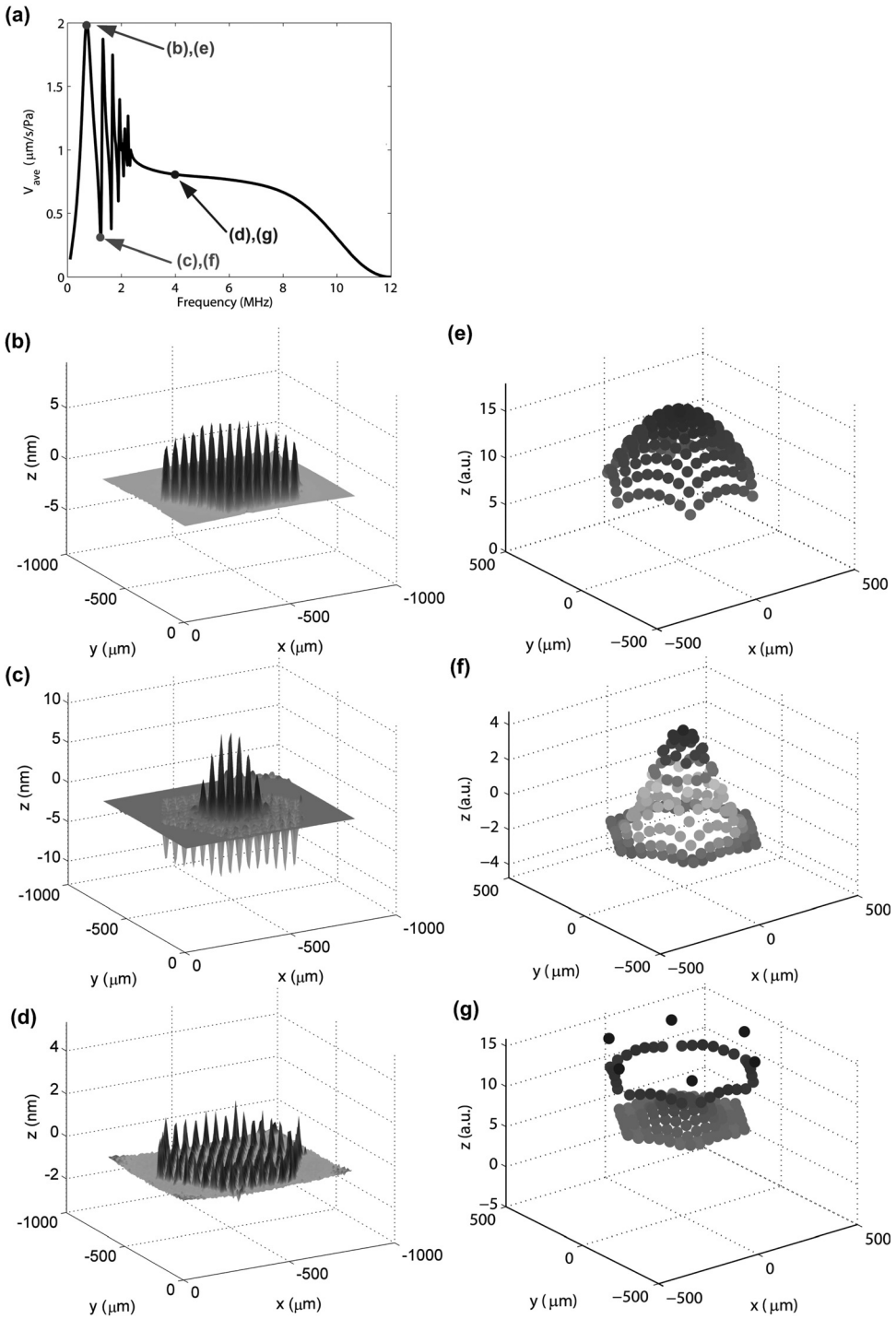

FIG. 8. (a) The frequencies of the displacement measurements depicted on the frequency response of average velocity of the plates. The measured displacement of the fabricated device in Fig. 7 in immersion with an excitation frequency of (b) 0.7 MHz, (c) 1.26 MHz, and (d) 4 MHz. The calculated displacement pattern of device B at corresponding frequencies: (e) 0.67 MHz, (f) 1.3 MHz, and (g) 4 MHz.

phase; and they generate sound waves in the medium above the plates.

The dynamic responses of the plates are measured by a laser Doppler vibrometer (LDV). The device is immersed in vegetable oil, which is electrically insulating but still has similar acoustic properties to water, and actuated by an AC signal at an excitation frequency. The LDV measures the displacement response in time domain at a specific location of the transducer. By changing the location of the measurement spot (using XY stage), dynamic response of all plates can be extracted, as shown in Fig. 8. The fabricated device is measured at three frequencies, which are depicted in Fig. 8(a). The first frequency is the fundamental frequency of the flexible-transducer mode (0.67 MHz), at which point all the plates are moving in the same phase. The second frequency is 1.26 MHz, at which the first local minimum of the average velocity is observed. The third frequency is the frequency of the inflexible-transducer mode (4 MHz). The snapshots of measured displacement in Figs. 8(b), 8(c), and 8(d) represent the mode shape of the transducer array and they display agreement with the results from analytic calculation [Figs. 8(e), 8(f), and 8(g)] and the snapshot of the FEA [Figs. 6(a), 6(b), and 6(d)].

The complex shapes of the transducer at frequencies in the flexible-transducer mode have been observed previously.[9,10,12] However, they focused on 1-D linear array, which has only a few vibrating plates along the width of the unit transducer. Due to the limited number of the plates along the direction of interest, the previous work presented that the complex shape existed but did not clearly show the out-of-phase motion of the transducer. The transducers in this work have a large aperture size and several shapes of motion as shown in Figs. 6 and 8. Therefore, it is worthy to evaluate the pressure distribution in both near-field and far-field as an extension of the investigation on the complex motions of the transducer.

IV. PRESSURE RESPONSE

A. Near-field pressure distribution

The response shape of the transducer array made up of multiple flexural plates is different from the mode shape of a piston transducer. In the flexible-transducer mode, the transducer array behaves like a suspended hexagonal resilient disk and presents an out-of-phase vibration motion at several frequencies. In the inflexible-transducer mode, most of the plates vibrate in-phase, except the edge plates have a phase delay with respect to the inner plates. Therefore, the distribution of generated sound wave should not be similar to that of conventional piston transducers.

In order to evaluate the near-field pressure distribution, the pressure of the device B is calculated by Rayleigh integral method,[17] based on the velocity responses of all plates in Fig. 4. The calculation is performed on the area depicted in Fig. 9(a) at five frequencies: three frequencies in the flexible-transducer mode (0.789 MHz, 1.232 MHz and 1.674 MHz) and two frequencies in the inflexible-transducer mode (3.2 MHz and 6.13 MHz), as depicted in Fig. 9(b).

The calculated pressure distributions of the device B at the five frequencies are presented in Figs. 10(a)–10(e). Note that the pressure level is normalized by $P_0 = \sum_{i=1}^{N} v_i/N \cdot Z_0$. For the sake of comparison, the pressure distributions of a piston transducer, with the same effective radius and operating frequency, are calculated. The piston transducer has a radius of the effective radius (r_{eff}) on the device B [shown as the biggest circle in Fig. 2(b)] and has the velocity of $v_{ave} = \sum_{i=1}^{N} v_i/N$. The calculated pressure fields of the piston transducer are normalized and plotted in Figs. 10(f)–10(j).

The comparisons shown in Fig. 9 clearly indicate the characteristics of the near-field pressure of a multi-plate transducer. In the flexible-transducer mode, there are dramatic variations of pressure on the surface of the transducer. In particular, at 1.232 MHz and 1.674 MHz, the level of the surface pressure is much higher than P_0. However, the pressure is rapidly cancelled out in further fields [Figs. 10(b) and 10(c)]. In the inflexible-transducer mode, the dramatic variations of the surface pressure disappear and the surface pressure converges to P_0 [Figs. 10(d) and 10(e)]. Although the mode is named as the inflexible-transducer mode, the surface pressure distribution of the mode is different to that of the piston transducer in Figs. 10(i) and 10(j); in a typical piston transducer, there are fluctuations of the surface pressure ranging from 0 to $2 \times P_0$. The near-field pressure distribution of the multi-plate transducer is similar to that of a resilient plate; Mellow[18] presented the analytic solution of the pressure distribution of a circular resilient disk, which has a uniform surface pressure.

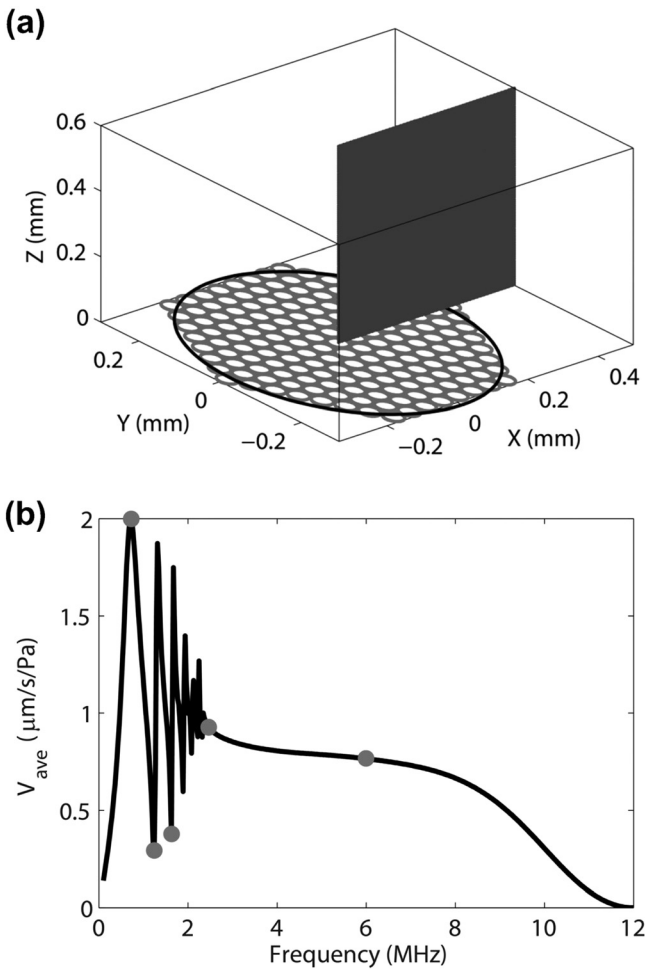

FIG. 9. (a) The 3-D view of the calculation area for near-field pressure distribution. (b) The selected frequencies (dots) for the pressure calculation.

B. Far-field pressure

In the actual applications of transducers, the far-field radiation pattern is more important than the near-field pattern. Therefore, in order to examine the differences in the far-field, the radiation pressure pattern in the far-field is calculated along the arc line, which is equidistant from the center of the transducer. The distance between the transducer and the point of calculation (z) is 25 mm, at which the Fresnel parameter, S ($S = z\lambda/r_{eff}^2$) is more than 1 (i.e., far-field). When z = 25 mm, S is 4000 at 0.1 MHz and 33 at 12 MHz. At each frequency, the pressures along the equidistant line are calculated by Rayleigh integral and normalized to the maximum pressure in the line to present the normalized radiation pattern.

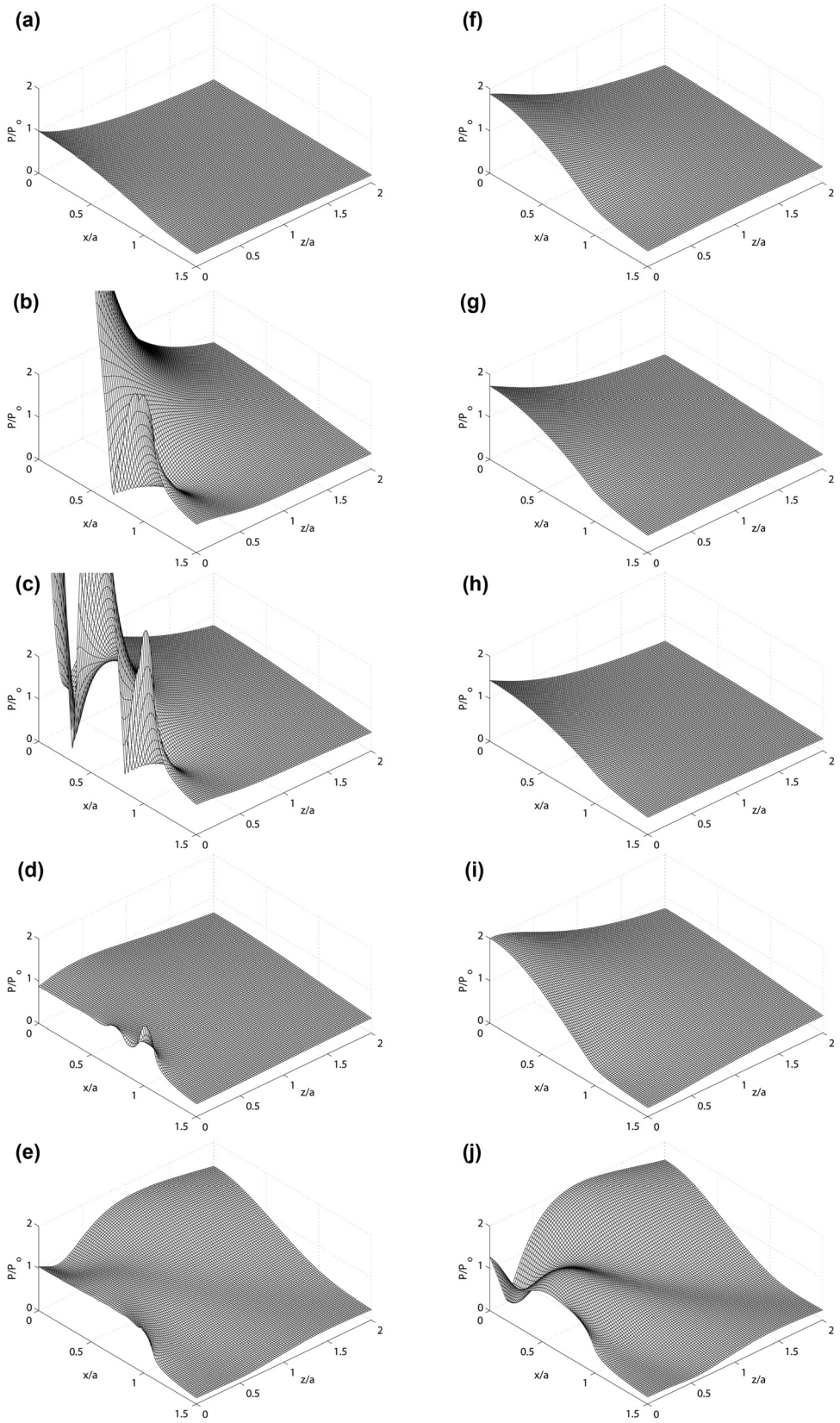

FIG. 10. (left) The near-field pressure distributions of the CMUT and (right) the piston transducer. The excitation frequencies are (a and f) 0.789 MHz, (b and g) 1.232 MHz, (c and h) 1.674 MHz, (d and i) 3.2 MHz, and (e and j) 6.13 MHz.

Figure 11 presents the radiation patterns of the piston transducer and the CMUT of the same effective radius at wide range of frequency. The piston transducer [Fig. 11(a)] and the CMUT [Fig. 11(b)] have the similar radiation patterns at high frequencies (more than 3 MHz), which correspond to the inflexible-transducer mode; both transducers present similar location of the null, at which the pressure has a local minimum. On the contrary, in the flexible-transducer mode (low frequency), there are several frequencies at which the pattern of the CMUT significantly differs from that of the piston transducer [see Fig. 11(c)]; the CMUT presents the out-of-phase motion at these frequencies as shown in Fig. 6.

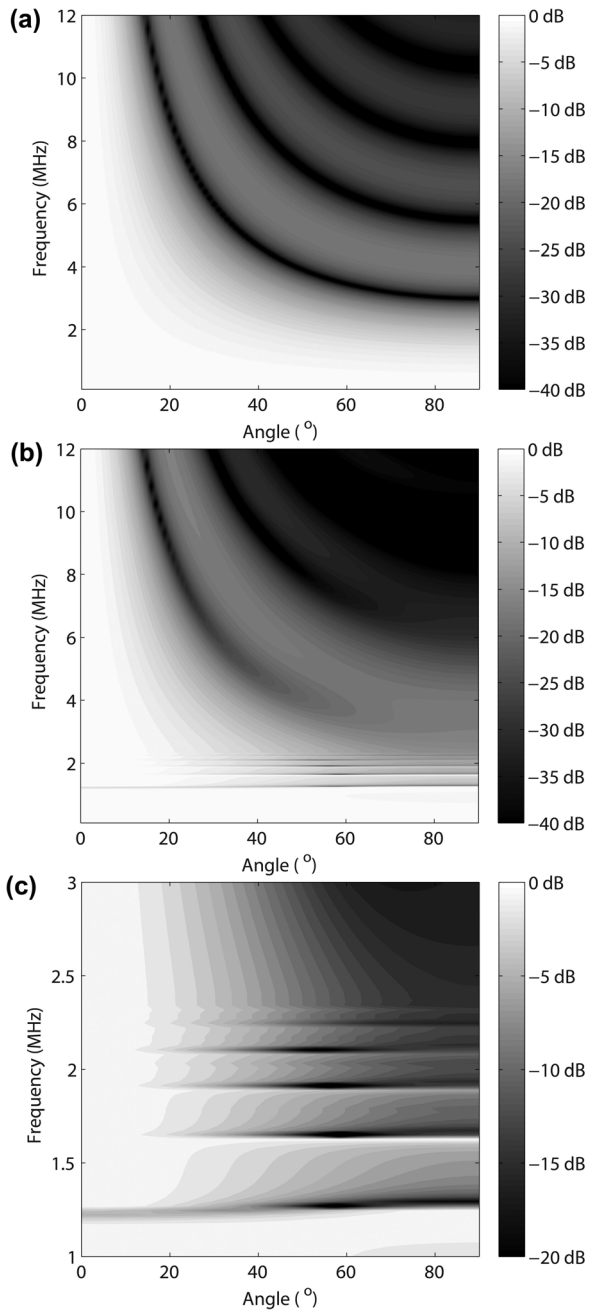

FIG. 11. The far field radiation pattern of (a) the piston transducer (0.1–12 MHz), (b) CMUT in wide range of frequencies (0.1–12 MHz), and (c) the CMUT in narrow range of frequencies (1–3 MHz). The distance from the center of the transducer to the point of the calculation is 25 mm.

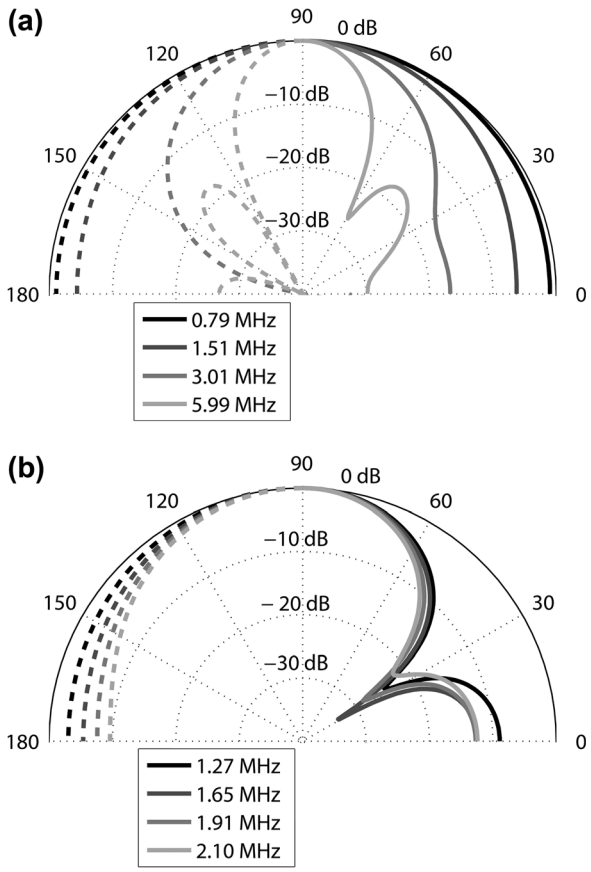

FIG. 12. Radiation patterns of the CMUT (solid line) and the piston transducer (dotted line) (a) at several frequencies at which two transducers present similar patterns and (b) at several frequencies at which the CMUT presents out-of-phase motion. The distance from the center of the transducer to the point of the calculation is 25 mm.

In order to exam the radiation patterns of two transducers, several frequencies are selected, and the radiation patterns at those frequencies are plotted in a polar coordinate (Fig. 12). When the CMUT presents the out-of-phase motion, the radiation patterns of the CMUT show strong nulls, which locate at 60° from the on-axis as shown in Fig. 12(b). Due to the nulls, the CMUT presents a more directive radiation pattern than the piston transducer. Except these frequencies, similar radiation patterns are observed in both the piston and the CMUT [Fig. 12(a)]. Please note that, the CMUT has weaker destructive interference than the piston transducer, and the radiation does not go to zero at the nulls [Fig. 12(a)].

V. DISCUSSION

The main application of the calculation method is to estimate the performance of multi-plate transducers, including CMUTs. The advantage of the proposed method is that it allows incorporation of the following three considerations: (1) estimation of the parallel resonant frequency of a plate and utilizing it in the frequency response calculation, (2) calculations based on an arbitrary number of plates at arbitrary locations, and (3) prediction of the location of the null frequencies at which the average velocity becomes local minima. Additionally, the calculation method proposed in this paper can be expended to include the calculation of the pressure response and the input impedance of a transducer. It is especially important to estimate the null frequency in the design step as it has major influence on the 3-dB bandwidth of the transducer.

There are several comments on the assumptions in the Sec. II A. The assumption (2) implies the electrical boundary conditions of all plates are identical to each other. In general, the same excitation voltage is applied to all plates and the applied voltage is not dependent on the location of the plates. The uniformly distributed electrostatic force on the plate is valid when the deflection of the plate is much smaller than the effective gap height between the two electrodes (i.e. top electrode and the substrate).

Assumption (3) was necessary in order to develop the calculation method presented in this paper. Porter[5] defined the acoustic radiation impedance as

$$Z_{11} = \frac{1}{\pi r^2 \langle |u| \rangle^2} \int_0^{2\pi} \int_0^r P(r_0) u^*(r_0)\, r_0 dr_0 d\phi, \tag{12}$$

whereas Mason[13] defined the acoustic impedance as the ratio of the mean pressure to the mean velocity of the plate. When the pressure on the plate is uniform, these two definitions give the same result. In addition, the pressure non-uniformity on the plate did not significantly affect the velocity profile of the plate as shown in the FEA results in Figs. 5 and 6. As shown in Figs. 5(d) and 6(d), the non-uniformity of the acoustic pressure starts to alter the velocity profiles of some plates. However the effect is limited for the edge plates at the high frequency.

All the calculations in this paper assume a quasi-CW operation. The model assumes that the CW excitation is applied on the transducer and the transducer is in steady-state condition in the amplitude and phase of the oscillation. These assumptions enable Eq. (11), which assumes that one plate interacts with all neighboring plates. Thereby, if the size of the transducer is larger than the wavelength of the sound inside the medium, the estimation of the dynamic behavior of multi-plate transducer in the first few cycles of burst signal is out of the scope of the calculation method. On the contrary, the predictions of a CW-mode operation of the device, such as high intensity focused ultrasound (HIFU) operation, or a quasi-CW operation of an ultrasound transducer array, fall into the applicable range of this calculation.

The near-field pressure distributions show that CMUTs are different from piston transducers. At the null frequency in the flexible-transducer mode, the plate responses distort the pressure pattern from the near field to the far field. Even in the inflexible-transducer mode, as shown in Figs. 10(d) and 10(e), the pressure on the surface of the CMUT is more uniformly distributed around P/P_0 and the distribution is more similar to the circular resilient disk[18] than the piston transducer. Additionally, Fig. 10(e) does not present the rapid changes of pressure in the Fresnel zone as shown in Fig. 10(j). Therefore, the CMUT may not be considered as a piston transducer in both the flexible-transducer mode and the inflexible-transducer mode in the near-field pressure calculation.

VI. CONCLUSION

This paper presents a method used to calculate the dynamic response of a multi-plate acoustic transducer. The velocity responses of many plates are calculated in the frequency domain based on the acoustic impedance of the plate and the mutual acoustic impedance from the neighboring plates. The calculation method is validated by FEA and the measurement of a fabricated CMUT immersed in liquid. This multi-plate transducer presents two operating conditions: (1) the flexible-transducer mode in the low frequency range and (2) the inflexible-transducer mode in the high frequency range. In the flexible-transducer mode, the mode shape of the transducer is similar to that of the suspended plate, whereas, in the inflexible-transducer mode, the mode shape is similar to that of a piston. The pressure distribution of the inflexible-transducer mode is similar to that of a single resilient disk.

This calculation method can be used as an alternative tool over FEA to calculate the mechanical response of multi-plate transducers, including CMUTs. The computation time of the proposed method is much faster than the FEA, and thus, design optimization and studies of various multi-plate transducers can be performed significantly faster. In addition, this calculation method can be incorporated into the calculation of other key parameters of transducers, including output pressure response, and fractional bandwidth. The multi-plate transducers show the null frequencies, at which the average velocity becomes locally minimum. The prediction of the null frequencies is an important feature of the calculation method. In the design step of the transducer, the null frequency should be moved away from the operating frequency in order to maintain an appropriate mode and sustain wide bandwidth.

ACKNOWLEDGMENTS

This work is supported by the National Institute of Health under Grant 5R01CA134720. This work was performed, in part, at the Stanford Nanofabrication Facility (a member of the National Nanotechnology Infrastructure Network); which is supported by the National Science Foundation under Grant ECS-9731293.

APPENDIX

The parallel resonant frequency, f_p, is defined as the frequency at which the average velocity of the plate reaches a local minimum.[11] In the case of the circular plate without medium, the parallel resonant frequency is calculated by solving the differential equation, which describes the acoustic impedance of the circular plate[13]:

$$Z_m = \frac{p}{\upsilon} = j\omega\rho_m t \left[\frac{\left[k_2 \frac{J_0(k_1 r)}{J_1(k_1 r)} + k_1 \frac{I_0(k_2 r)}{I_1(k_2 r)} \right] \frac{k_1 k_2 r}{2(k_1^2 + k_2^2)}}{\left[k_2 \frac{J_0(k_1 r)}{J_1(k_1 r)} + k_1 \frac{I_0(k_2 r)}{I_1(k_2 r)} \right] \frac{k_1 k_2 r}{2(k_1^2 + k_2^2)} - 1} \right], \tag{A1}$$

where p is the applied pressure on the plate; J_0 and J_1 are Bessel functions; I_0 and I_1 are modified Bessel functions. k_1 and k_2 are given by

$$k_1 = \sqrt{\frac{\sqrt{d_T^2 + 4c_T\omega^2} - d_T}{2c_T}}, \; k_2 = \sqrt{\frac{\sqrt{d_T^2 + 4c_T\omega^2} + d_T}{2c_T}}$$
$$c_T = \frac{(E+T)t^2}{12\rho_m(1-\nu^2)}, \; d_T = \frac{T}{\rho_m t}, \tag{A2}$$

where T is the tension along radial direction.

The fundamental frequency of the plate, f_1, corresponds to the radian frequency at which the numerator of Eq. (A1) becomes zero. At the parallel resonant frequency, the denominator of Eq. (A1) becomes zero. In general, the ratio between the parallel resonant frequency and the fundamental frequency, f_p/f_1 is 3.4.

However, there is no closed-form solution of the fundamental frequency and the parallel resonant frequency of the circular plate loaded with medium. In the case of water medium, Lamb presented the fundamental frequency of the circular plate in contact with water as[19]

$$f_{1,\text{load}} = \frac{f_1}{\sqrt{1+\beta}}, \quad \beta = 0.6689\frac{\rho}{\rho_m}\frac{r}{t}. \tag{A3}$$

The effect of water is virtually to increase the inertia of the plate in the ratio of $1+\beta$. However, the increase of the inertia by the factor does not proportionally reflected on the changes of the f_p. Based on the finite element analysis of plates with various dimensions, density, and stiffness, the f_p/f_1 of the water-loaded plates shows a constant value, 5.5; the parallel resonant frequency of the water-loaded circular plate is approximately

$$f_{n,\text{load}} \approx 5.5\frac{f_1}{\sqrt{1+\beta}}. \tag{A4}$$

[1]T. Hueter, "Twenty years in underwater acoustics: Generation and reception," J. Acoust. Soc. Am. **51**, 1025–1040 (1972).
[2]R. L. Pritchard, "Mutual acoustic impedance between radiators in an infinite rigid plane," J. Acoust. Soc. Am., **32**, 730–737 (1960).
[3]C. H. Sherman, "Analysis of acoustic interactions in transducer arrays," IEEE Trans. Son. Ultrason., **13**, 9–15 (1966).
[4]R. New and T. Eisler, "Acoustic radiation from multiple spheres," J. Sound Vib. **22**, 1–17 (1972).
[5]D. T. Porter, "Self-and mutual-radiation impedance and beam patterns for flexural disks in a rigid plane," J. Acoust. Soc. Am., **36**, 1154–1161 (1964).
[6]H. Lee, J. Tak, W. Moon, and G. Lim, "Effects of mutual impedance on the radiation characteristics of transducer arrays," J. Acoust. Soc. Am. **115**, 666–679 (2004).
[7]B. Froelich, "Theoretical model for circular benders in a rigid baffle and radiating in fluid," J. Acoust. Soc. Am., **84**, 822–829 (1988).
[8]M. Greenspan, "Piston radiator: Some extensions of the theory," J. Acoust. Soc. Am., **65**, 608–621 (1979).
[9]S. Ballandras, M. Wilm, W. Daniau, A. Reinhardt, V. Laude, and R. Armati, "Periodic finite element/boundary element modeling of capacitive micromachined ultrasonic transducers," J. Appl. Phys. **97**, 034901 (2005).
[10]A. Caronti, A. Savoia, G. Caliano, and M. Pappalardo, "Acoustic coupling in capacitive microfabricated ultrasonic transducers: Modeling and experiments," IEEE Trans. Ultrason. Ferr. **52**, 2220–2234 (2005).
[11]M. N. Senlik, S. Olcum, H. Koymen, and A. Atalar, "Radiation impedance of an array of circular capacitive micromachined ultrasonic transducers," IEEE Trans. Ultrason. Ferr. **57**, 969–976 (2010).
[12]C. Meynier, F. Teston, and D. Certon, "A multiscale model for array of capacitive micromachined ultrasonic transducers," J. Acoust. Soc. Am. **128**, 2549–2561 (2010).
[13]W. Mason, *Electromechanical Transducers and Wave Filters*, 3rd ed. (D. Van Nostrand, New York, 1946), Chap 5, pp. 167–184.
[14]A. S. Ergun, G. G. Yaralioglu, and B. T. Khuri-Yakub, "Capacitive micromachined ultrasonic transducers: Theory and technology," J. Aerospace Eng. **16**, 76–84 (2003).
[15]A. S. Ergun, Y. Huang, X. Zhuang, O. Oralkan, G. G. Yarahoglu, and B. T. Khuri-Yakub, "Capacitive micromachined ultrasonic transducers: fabrication technology," IEEE Trans. Ultrason. Ferr. **52**, 2242–2258 (2005).
[16]K. K. Park, H. J. Lee, M. Kupnik, and B. T. Khuri-Yakub, "Fabrication of capacitive micromachined ultrasonic transducers via local oxidation and direct wafer bonding," J. Microelectromech. S. **20**, 95–103 (2011).
[17]G. S. Kino, *Acoustic Waves: Devices, Imaging, and Analog Signal Processing* (Prentice-Hall, Englewood Cliffs, 1987), Chap. 3, pp. 156–163.
[18]T. Mellow, "On the sound field of a resilient disk in free space," J. Acoust. Soc. Am. **123**, 1880–1891 (2008).
[19]H. Lamb, "On the vibrations of an elastic plate in contact with water," Proc. R. Soc. London, Ser. A **98**, 205–216 (1920).